

Cloud Detection with MODIS. Part II: Validation

S. A. ACKERMAN, R. E. HOLZ, AND R. FREY

Cooperative Institute for Meteorological Satellite Studies, Space Science and Engineering Center, University of Wisconsin—Madison, Madison, Wisconsin

E. W. ELORANTA

Space Science and Engineering Center, University of Wisconsin—Madison, Madison, Wisconsin

B. C. MADDUX

Department of Atmospheric and Oceanic Science, University of Wisconsin—Madison, Madison, Wisconsin

M. MCGILL

NASA Goddard Space Flight Center, Greenbelt, Maryland

(Manuscript received 20 August 2007, in final form 6 December 2007)

ABSTRACT

An assessment of the performance of the Moderate Resolution Imaging Spectroradiometer (MODIS) cloud mask algorithm for *Terra* and *Aqua* satellites is presented. The MODIS cloud mask algorithm output is compared with lidar observations from ground [Arctic High-Spectral Resolution Lidar (AHSRL)], aircraft [Cloud Physics Lidar (CPL)], and satellite-borne [Geoscience Laser Altimeter System (GLAS)] platforms. The comparison with 3 yr of coincident observations of MODIS and combined radar and lidar cloud product from the Department of Energy (DOE) Atmospheric Radiation Measurement (ARM) Program Southern Great Plains (SGP) site in Lamont, Oklahoma, indicates that the MODIS algorithm agrees with the lidar about 85% of the time. A comparison with the CPL and AHSRL indicates that the optical depth limitation of the MODIS cloud mask is approximately 0.4. While MODIS algorithm flags scenes with a cloud optical depth of 0.4 as cloudy, approximately 90% of the mislabeled scenes have optical depths less than 0.4. A comparison with the GLAS cloud dataset indicates that cloud detection in polar regions at night remains challenging with the passive infrared imager approach.

In anticipation of comparisons with other satellite instruments, the sensitivity of the cloud mask algorithm to instrument characteristics (e.g., instantaneous field of view and viewing geometry) and thresholds is demonstrated. As expected, cloud amount generally increases with scan angle and instantaneous field of view (IFOV). Nadir sampling represents zonal monthly mean cloud amounts but can have large differences for regional studies when compared to full-swath-width analysis.

1. Introduction

What is a cloud? According to the American Meteorological Society's *Glossary of Meteorology*, a cloud is "a visible aggregate of minute water droplets and/or ice particles in the atmosphere above the earth's surface."

Corresponding author address: Steven A. Ackerman, CIMSS, University of Wisconsin—Madison, 1225 W. Dayton St., Madison, WI 53706.
E-mail: stevea@ssec.wisc.edu

From the perspective of remote sensing, the application and the instrument determine the answer. What is considered a cloud in one application may be defined as clear in another. For example, detection of thin cirrus clouds is important for infrared remote sensing of sea surface temperature (SST) and climate but is of little concern for microwave remote sounding of atmospheric temperature. This paper focuses on clear- versus cloudy-sky discrimination using passive reflected solar and infrared observations from the National Aeronautics and Space Administration (NASA) Earth

Observing System (EOS) *Terra* and *Aqua* polar-orbiting satellites, in particular, the Moderate Resolution Imaging Spectroradiometer (MODIS) (Barnes et al. 1998). Developed in collaboration with members of the MODIS science team, the MODIS cloud screening approach includes new approaches while still incorporating many previously existing techniques to detect obstructed fields of view (Ackerman et al. 1998).

Part I (Frey et al. 2008) of this paper summarizes the recent improvements to the cloud mask detection algorithm. Here (Part II), we provide an assessment of cloud detection capability of the MODIS cloud mask algorithm in the MODIS instantaneous field of view (IFOV; Ackerman et al. 1998). The assessment is primarily made through comparisons of MODIS results with observations from active sensors. Measurements from passive imaging satellite systems provide a long time series of global observations; however, understanding the constraints in cloud detection from these measurements is required to ensure proper interpretation of existing and future cloud datasets. In this context, we make use of MODIS observations to investigate the sensitivity of cloud detection to the various spatial and spectral constraints of the instrument. Thresholds are chosen to discriminate between clouds and clear sky but may vary according to view angle, surface type, time of year, or solar zenith angle. We demonstrate the sensitivity of cloud detection to various thresholds and the impacts on derived global cloud amount. We also consider the impacts of IFOV and sampling strategies on derived cloud amount. Some comparisons to existing satellite cloud datasets are presented here, but a separate paper will provide detailed comparisons of MODIS cloud products with those derived from other satellites. Finally, this paper does not assess the detection capability for all scene types. For example, in the comparison with the land-based active sensors, sun glint does not become an issue as noted in the study of Zhao and Di Girolamo (2006).

2. Global view of MODIS cloud amount

Figure 1 shows the global distribution of cloud amount derived from MODIS from both *Terra* and *Aqua* satellites. As expected, the large-scale patterns are similar to other satellite datasets of cloud amount (Rossow 1989, Rossow et al. 1993; Thomas et al. 2004; Wylie et al. 1994). The intertropical convergence zone (ITCZ) is clearly evident as are the subtropical high pressure systems and the marine stratocumulus regions. While there are differences in the performance between the two instruments, the algorithms are essentially the same. Therefore, the differences result from

either instrument performance or diurnal variations in cloud amount. Globally, results between the two satellites are offset by about 2%, with *Terra* greater than *Aqua* in the long-term mean.

Figure 2 shows the differences between MODIS *Aqua* and *Terra* monthly mean daytime cloud fractions for August 2002 through July 2007. These plots show *Aqua* minus *Terra*, (i.e., 1330 minus 1030 local time) values. Whether the differences in cloud amount are due to threshold differences, calibration differences, or instrument differences—or if they are real—are difficult to completely assess. The *Aqua* $R_{0.86}$ ocean cloud thresholds are higher than those of *Terra* due to observed clear-sky differences in reflectance; however, threshold differences would yield a consistent bias in cloud amount, while the differences shown in Fig. 2 are not biased in this way and do contain expected variations in geographic regions characterized by specific cloud regimes. For example, over ocean surfaces, *Aqua* generally has a greater cloud fraction, with the notable exception over the marine stratocumulus regions.

Because of the diurnal variation in stratocumulus (Minnis and Harrison 1984; Minnis et al. 1992), it is expected that *Terra* and *Aqua* cloud amounts in regions of stratocumulus will vary with a seasonal dependence on the magnitude. The difference is greater in the Peruvian and Namibian regions in December and March than during June and September. Static stability reaches a maximum in these regions during September–November (Klein and Hartmann 1993) leading to smaller diurnal variations. During December, the Peruvian stratus deck is seen to erode most along the edges between *Terra* and *Aqua* observation times. At the center of the cloud deck, where the marine boundary inversion would be climatologically the strongest, the differences between *Aqua* and *Terra* are at a minimum. Generally, convective regions over land show greater cloud amounts in the afternoon as detected by *Aqua*. There are interesting differences in polar regions during the equinox months. In March, *Terra* detects more cloud at both poles, while in September *Aqua* observes more cloud in the Arctic.

The 3-h difference between the *Terra* and *Aqua* MODIS data results in global differences on the order of a couple of percent, while regional studies have demonstrated differences of up to 20%. This comparison, contrasting cloud amounts from essentially the same instrumentation and algorithm, demonstrates expected variations in the cloud field and encourages us to treat the two satellite products as similar datasets. The next section explores differences that can result from selection of spectral thresholds.

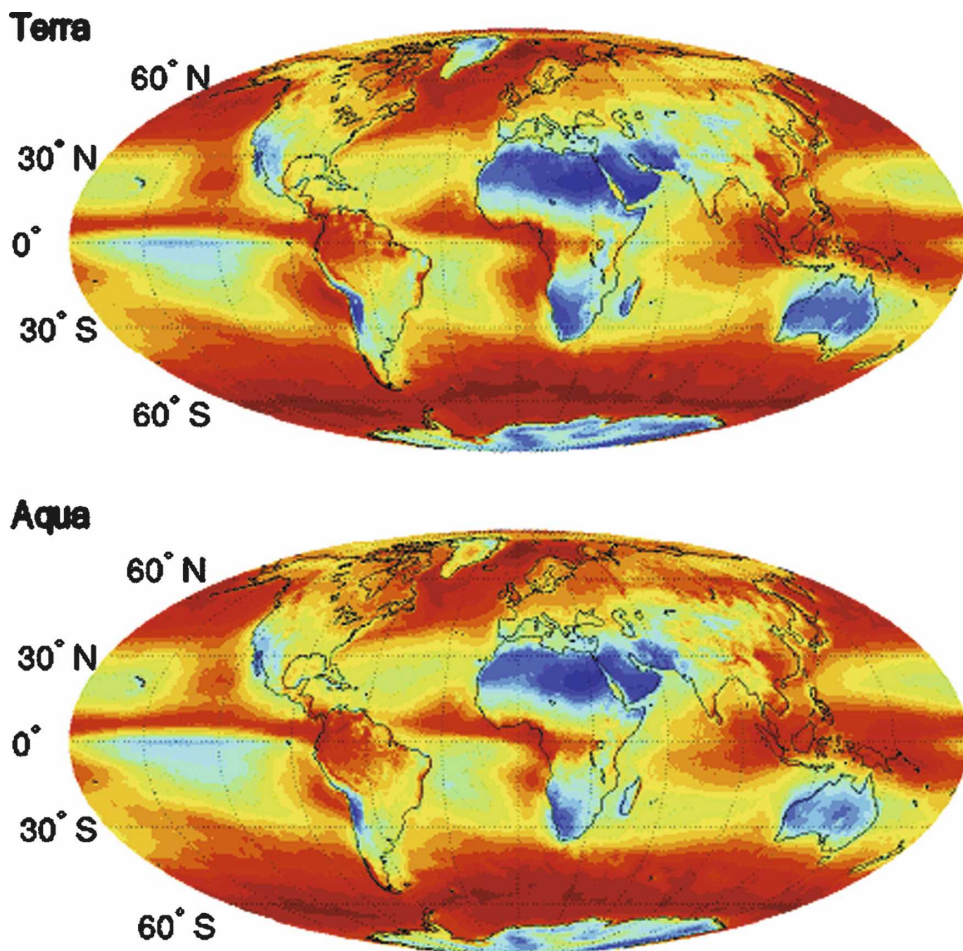


FIG. 1. The mean daytime cloud fractions for (top) *Terra* and (bottom) *Aqua* for August 2002 through July 2007. Overall, these cloud patterns across much of the globe are similar.

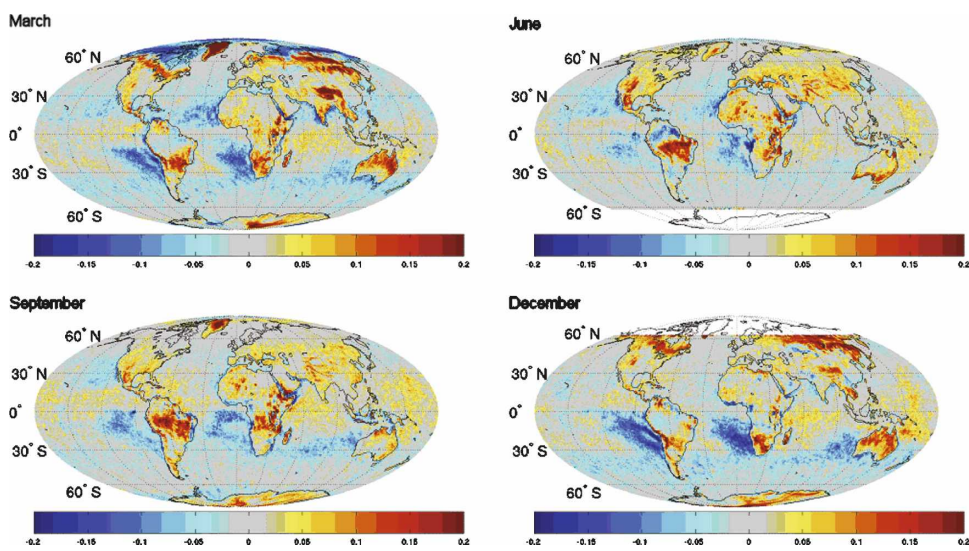


FIG. 2. The images show MODIS *Aqua* minus *Terra* monthly mean daytime cloud fraction for 5 yr (August 2002–July 2007) for March, June, September, and December.

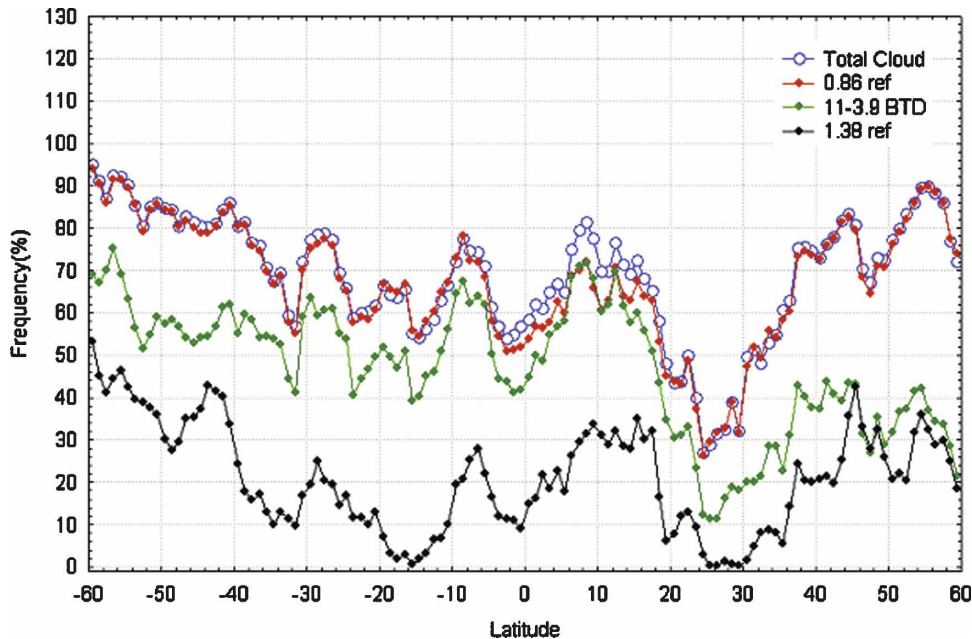


FIG. 3. Zonal mean frequencies of cloudy conditions for 16 Oct 2003, daytime ocean scenes as a function of three threshold cloud detection tests, and the combination of all 16 tests from MODIS.

3. Cloud detection

Cloud detection is fundamentally a function of the contrast between the target (cloud) and background environment (e.g., ground or atmosphere). The MODIS algorithm relies heavily on contrast in several spectral bands, assigning confidence thresholds to a series of spectral cloud tests (Ackerman et al. 1998; King et al. 2003; Platnick et al. 2003). In this section, we explore the sensitivity of cloud detection to specific spectral tests and instrument characteristics.

Figure 3 shows the zonal mean frequencies of cloud conditions in daytime ocean scenes on 16 October 2003 as functions of three cloud detection tests and the combination of all 16 tests from MODIS. Comparing the final results of the cloud mask with the individual tests shows that for this scene type, a single spectral test with the reflectance at $0.86 \mu\text{m}$ does very well alone. The largest error, only a few percent, occurs around 10°N . This single test works because of the high contrast between clear-sky and cloudy conditions and suggests that a comparison of different algorithms should include a comparison of this reflectance test alone to better understand any discrepancies among algorithms. We will use this result later to explore the sensitivity of cloud detection to a specific threshold and viewing geometry.

The $\text{BT}_{11} - \text{BT}_{3.9}$ difference test is not as sensitive to total cloud cover as the reflectance test. The daytime ocean threshold for assigning cloud to a pixel (outside

sun glint) is $\text{BT}_{11} - \text{BT}_{3.9} < -80.0 \text{ K}$. During the daylight hours the difference between BT_{11} and $\text{BT}_{3.9}$ is large and negative because of reflection of solar energy at $3.9 \mu\text{m}$. This technique has proven useful for detecting low-level water clouds. In addition, moderate to large differences between BT_{11} and $\text{BT}_{3.9}$ result when a nonuniform scene (e.g., broken cloud) is observed. These differences are due to the differential spectral responses of the two bands to varying scene temperatures as a result of Planck's law.

As expected, the $R_{1.38}$ threshold test underestimates the zonal mean cloud amount. While cloud tests using this MODIS channel detect low-level clouds in dry atmospheres, it is primarily sensitive to thick upper-level clouds. The MODIS cloud mask also has a thin cirrus detection algorithm that is not included in the overall results of the final cloud mask, but it is included as a separate result. The zonal fraction of thin cirrus detected by the $R_{1.38}$ channel, and not detected by any other tests, is shown in Fig. 4. This analysis indicates that very thin cirrus generally occupy less than 2% of most zonal regions.

The zonal mean frequencies of cloudy conditions for 16 October 2003 for nighttime ocean scenes as a function of three cloud detection tests and the combination of all nighttime tests from MODIS indicate that the multispectral mask (Fig. 5) is more sensitive than a single cloud test. This results from the lower contrast between cloud and clear sky at night. The best ap-

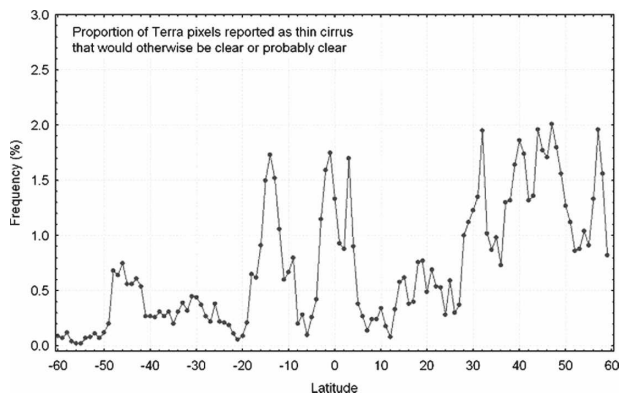


FIG. 4. Additional zonal mean cloud fraction due to thin cirrus using the 1.38- μm channel of *Terra* MODIS. Other tests in the algorithm indicate the pixel to be clear or probably clear.

proach seen here, which makes use of a brightness temperature difference between the observed BT_{11} and the estimated SST, still misses approximately 10% of the clouds.

Because the 0.86- μm reflectance test alone is capable of detecting nearly all the clouds over the ocean not affected by sun glint, it is useful to use this test to explore the sensitivity of cloud detection to a specific visible threshold. Figure 6 demonstrates this sensitivity for daytime ocean conditions equatorward of 60° and away from sun glint. The figure shows the 0.86- μm reflectance (x axis) versus the percentage of pixels greater than that value (e.g., cloud fraction if this reflectance was the threshold) as a function of MODIS viewing angle. As viewing geometries vary, cloud detection thresholds also vary (Minnis 1989). At low reflectances, a small change in the threshold can result in a large change in cloud amount. Because 100% of the pixels have a reflectance greater than 1%, if $R_{0.86} < 1\%$ were

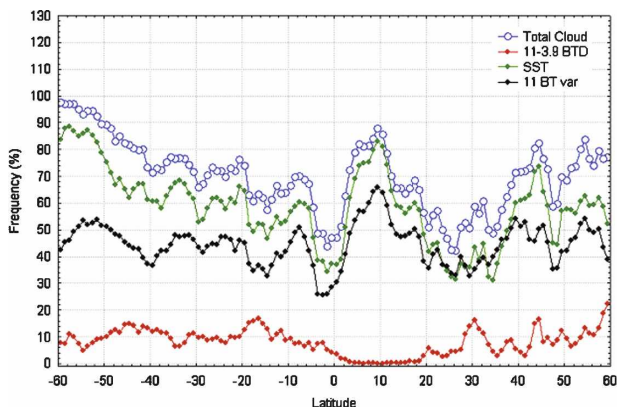


FIG. 5. Zonal mean frequencies of cloudy conditions for 16 Oct 2003, nighttime ocean scenes as a function of three cloud detection tests, and the combination of all tests (blue) from MODIS.

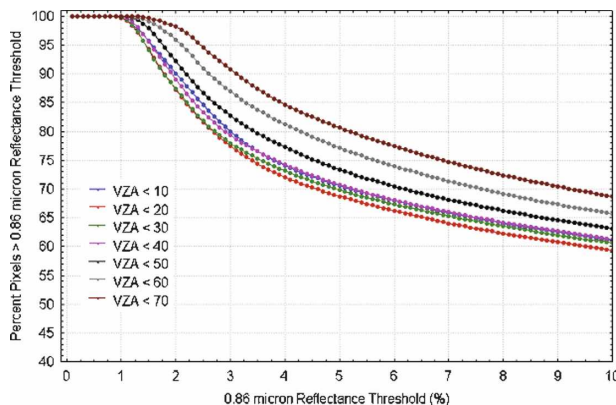


FIG. 6. The percentage of pixels with a reflectance at 0.86 μm greater than a given value for seven viewing zenith angles. *Aqua* MODIS data were collected on 1 Dec 2004 over ocean scenes outside of the sun-glint region.

set as the threshold for clear sky, all pixels would be labeled cloudy. While the thresholds are a function of view angle, the differences in derived cloud amount become more evident for view angles greater than about 40°. For a fixed reflectance of, say, 3%, more cloud would be derived for viewing angles greater than 40° compared to less than 40°. This behavior results from the reflectance properties of clouds, increased IFOV with view angle, and a parallax effect (cloud fraction within the IFOV will naturally increase with view angle). A decrease of the threshold from 5.5% to 4% would decrease the cloud fraction by approximately 5% for this particular test. The direct impact of any one test on the final result is ameliorated by the use of confidence levels and fuzzy logic in the MOD35 algorithm (Ackerman et al. 1998). The *Aqua* MODIS thresholds for this test are 3.0%, 4.5%, and 6.5% for 1.0, 0.5, and 0.0 confidence of clear sky, respectively.

As a final test of the sensitivity of cloud detection to a particular threshold, we varied the MODIS band 1 and 2 reflectances ($R_{0.66}$ and $R_{0.86}$, respectively) and the threshold of the 0.86-/0.66- μm ratio test to explore the global impact on the derived total cloud amount (Table 1). The tests were performed on daytime *Terra* data collected on 1 April 2003 between 60°N and 60°S. It is found that the impact is small with a change in cloud amount of less than 1%, except for ocean scenes, where the effect is slightly greater than 2%.

Satellite imager IFOVs are not always completely cloudy or clear, so that cloud edges and subpixel-scale clouds can cause ambiguity when defining appropriate thresholds (Di Girolamo and Davies 1997). Because many clouds are organized into spatially nonrandom systems by radiative and dynamic processes in the atmosphere, a higher proportion of larger IFOVs contain

TABLE 1. Cloud amount (60°S–60°N) as a function of reflectance biases and reflectance thresholds.

	Cloud amount
Collection 5 cloud mask	Water 72.7% Land 54.1%
Increase all B1 and B2 reflectance by 5% of the original	Water 73.3% Land 54.6%
Decrease all B1 and B2 reflectance by 5% of original	Water 72.2% Land 53.6%
Increase VIS/nadir reflectance test threshold by 1%	Water 70.7% Land 54.1%
Decrease VIS/nadir reflectance test threshold by 1%	Water 75.5% Land 54.7%

cloud edges and subpixel clouds than do smaller IFOVs. To explore the impact of IFOV size on cloud detection, clear-sky fractions were determined by increasing the MODIS IFOV from 1 km to larger groupings (e.g., 2 km on a side, 4 km on a side, etc.), but cloud test thresholds were held constant. To be classified as clear in this analysis, all MODIS pixels within a group were required to be labeled as confidently clear or probably clear. Figure 7 shows the percentage of clear sky on 5 November 2000 as a function of these simulated footprint sizes. For the increased IFOV to be classified as clear, the reflectance has to satisfy the threshold set by the 1-km pixel so the clear-sky amounts rapidly decrease with increasing footprint size. The value in a 6-km IFOV is typically half that of a 1-km IFOV. IFOV size has a large impact on observed cloud amounts due to subpixel cloud fields. The subpixel effects can be ameliorated in an algorithm by modifying the clear-sky threshold. Because IFOV size has a large impact on observed cloud amounts, care should be taken when comparing cloud fraction from sensors with differing IFOV sizes.

Instrument swath widths also impact estimates of global cloud amount distributions. To explore this impact on zonal clear-sky amounts, we computed clear-sky fractions from 1-km MODIS observations during 16 October–15 November 2003 using only pixels within 1° of nadir (extreme nadir) and pixels within 20° of nadir. Figure 8 details differences in zonal mean clear-sky amounts during this period. As expected, the nadir sampling strategies result in greater clear-sky fractions, or less clouds, when compared to use of the entire swath width. Generally, the difference between the nadir views and the full swath is less than 5%. The impact of sampling is much larger on a regional scale as shown in Fig. 9, where differences in cloud amount for a 1° grid can differ by more than $\pm 30\%$. Thus, nadir and near-nadir viewing can produce similar zonal means but yield large differences regionally.

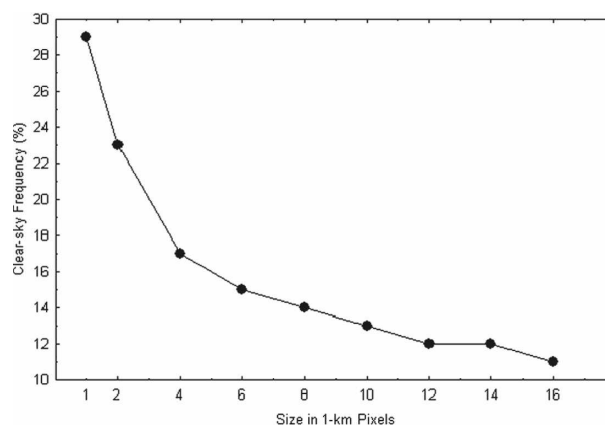


FIG. 7. The percentage of pixels labeled as confident clear or probably clear as a function of simulated pixel size using MODIS data collected on 5 Nov 2000.

The studies presented in this section provide insight into the sensitivity of the cloud mask algorithm results to instrument characteristics and algorithm thresholds. Awareness of this sensitivity is necessary for comparing the MODIS cloud detection to other observations covered in the next section.

4. Comparison with lidar/radar observations

a. Ground-based observations

The performance of the MODIS cloud mask has been addressed in several recent papers (King et al. 2003; Platnick et al. 2003; Lee et al. 2004; Li et al. 2007). In this section we compare MODIS cloud mask results with active sensors from ground, aircraft, and satellite platforms.

Three years (2003–05) of the Collection 5 cloud mask algorithm results were compared with those from the Department of Energy (DOE) Atmospheric Radiation Measurement (ARM) Program Active Remotely Sensed Cloud (ARSCL) product that combines ground-based observations from a micropulse lidar (MPL) and a millimeter-wavelength cloud radar (MMCR) to determine cloud presence and cloud-top heights (Clothiaux et al. 2000). This investigation utilizes the ARSCL retrievals at the Southern Great Plains (SGP) site in Lamont, Oklahoma (Stokes and Schwartz 1994).

The ARSCL algorithm processes and combines data from the MPL and MMCR to determine cloud-base and cloud-top altitude at a vertical spatial resolution of 45 m and a temporal resolution of 10 s. The ARSCL algorithm processes the four modes of MMCR operational output and merges it with the output of the MPL

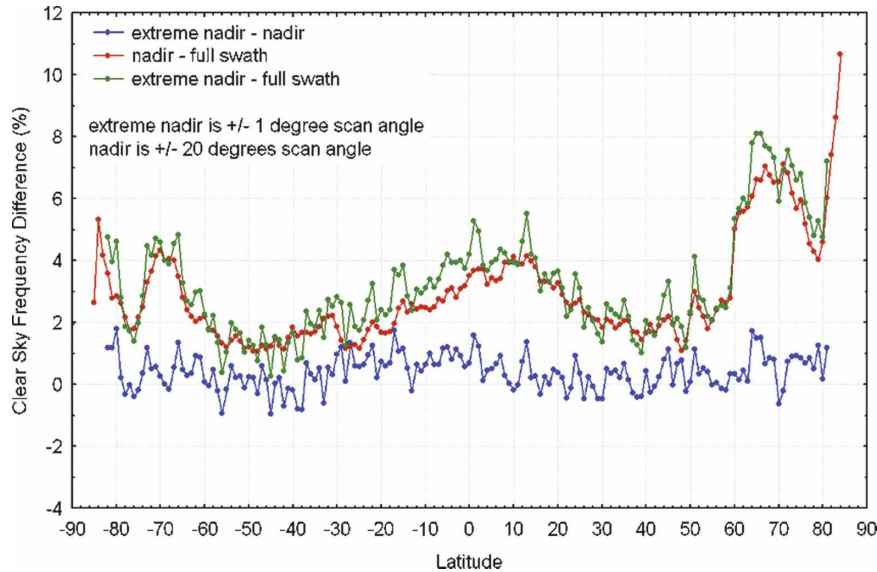


FIG. 8. Zonal mean differences in clear-sky frequency between three sampling strategies: full swath, nadir (within 20° of nadir), and extreme nadir (within 1° of nadir). Pixels with high-confidence clear or probably clear are considered clear in this study.

to produce cloud-top height retrievals. The present comparison with MODIS focuses on the cloud detection of the algorithm, using ARSCL cloud-top height retrieval only as an analysis tool.

Comparing cloud detection methods from two independent sources that retrieve cloud properties based on different physical principles over different spatial and temporal scales and viewing geometry makes for a difficult process. A group of 5×5 MODIS observations centered on the ARM site is used in the comparison, averaging the final cloud mask confidences (Ackerman et al. 1998) and assuming that a value of greater than 0.95 represents a clear scene. The radiances were collected from the MODIS direct broadcast system at the

University of Wisconsin—Madison and used as input to the Collection 5 MODIS cloud mask. The ARSCL cloud fraction is defined as the fraction of samples determined cloudy over a 30-min time period, with a cloud fraction of less than 5% considered to be clear.

Table 2 lists the comparison between the *Terra* and *Aqua* MODIS and the ARSCL cloud datasets. There is agreement between MODIS and ARSCL in approximately 83% of the collocated observations with little difference in skill score with season. Next, we explore cases when the two results differ and propose some possible causes.

First, we explore cases in which MOD35 flagged the scene as cloudy while the ARSCL dataset indicated

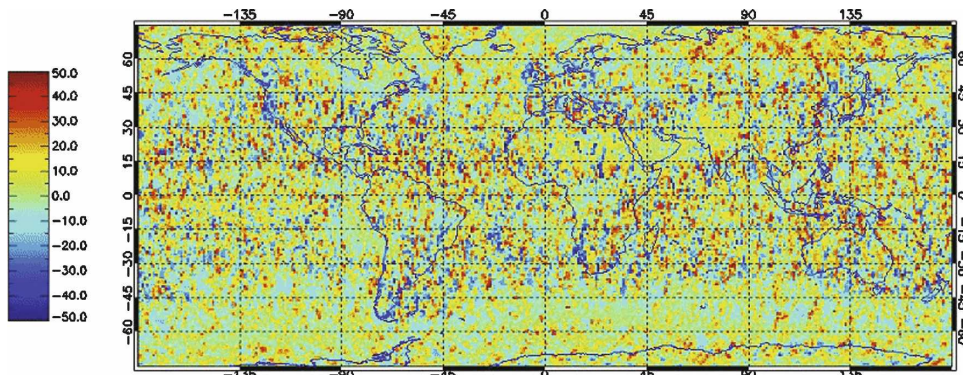


FIG. 9. The MODIS cloud mask minus the MODIS nadir-only cloud fraction from *Terra* MODIS from 16 Oct–15 Nov 2003.

TABLE 2. Comparison of MODIS cloud detection with the ARSCL over the ARM site of the SGP.

	ARCL clear	ARCL cloudy
MODIS clear	<i>Terra</i> : 146 <i>Aqua</i> : 117	<i>Terra</i> : 45 <i>Aqua</i> : 58
MODIS cloudy	<i>Terra</i> : 38 <i>Aqua</i> : 12	<i>Terra</i> : 298 <i>Aqua</i> : 185

clear. Figure 10 plots the average confidence level of these cases as a function of the standard deviation of the MODIS confidence level in the group of pixels around the ARM site. Those observations that are determined by MODIS as cloudy while ARSCL is indicating clear are mostly associated with the average MODIS confidence flag near 0.90 (Fig. 10), where we have defined a value of greater than 0.95 as clear. The low standard deviation indicates that the scenes are likely to be uniform, suggesting errors in the MODIS classification.

Those cases in which MODIS defines clear and ARSCL defines cloudy are explored in Fig. 11 by plotting the ARSCL cloud altitude versus the average ARSCL cloud fraction over the 30-min sampling period. Discrepancies occur for low cloud fractions, but these are not the majority of cases. Most differences occur for cloud-top altitudes greater than 8 km, suggesting that MODIS is missing some cirrus. The MODIS sensitivity to cirrus is greatest over the tropical waters and thick vegetation as the $R_{1.38}$ threshold can be set low and variations of the IR window surface emissivity are small. In the midlatitudes, lower water vapor amounts and spectral variations of the surface make detection of thin cirrus more difficult.

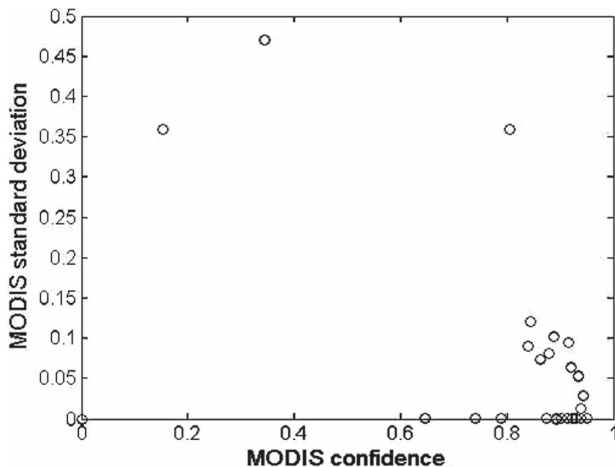


FIG. 10. MODIS average confidence level vs std dev for cases labeled by MODIS as cloudy and by the ARSCL algorithm as clear. The clear-sky confidence threshold is 0.95.

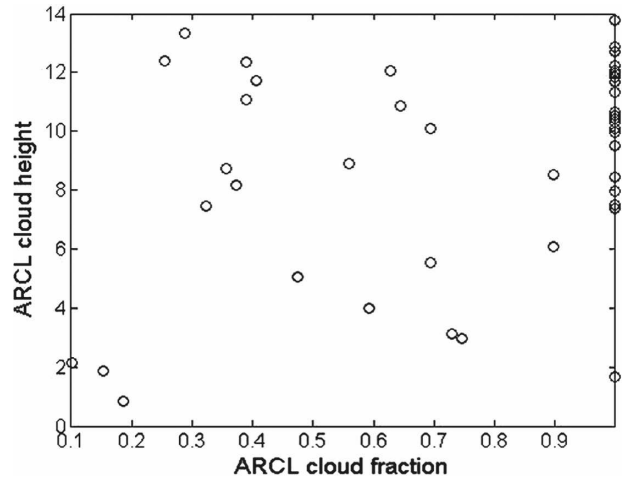


FIG. 11. ARSCL cloud fraction as a function of cloud height for those cases labeled as clear by the MODIS algorithm.

The difference in cloud detection rates for high clouds raises the issue of algorithm sensitivity to cloud optical depth. Next, we determine the minimum cloud optical depth that the MODIS algorithm can flag as cloudy.

b. Optical depth sensitivity

We take two independent approaches to estimating cloud optical detection limits: 1) compare observations of the MODIS Airborne Simulator (MAS) taken on board a high-altitude aircraft with coincident lidar observations and 2) compare cloud mask results from the MODIS cloud mask with ground-based measurements of visible optical depth from the Arctic High-Spectral

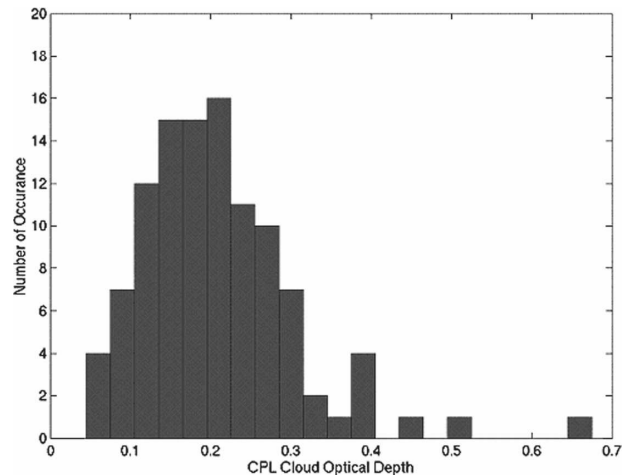


FIG. 12. The number of occurrences that a MAS pixel was identified as clear, but the CPL (McGill et al. 2002) detected a cloud with a given cloud optical depth.

TABLE 3. Comparison of MODIS cloud detection with the AHSRL over Madison.

	AHSRL clear	AHSRL cloudy
MODIS clear	39	133
MODIS cloudy	46	362

Resolution Lidar (HSRL). The MAS has a different IFOV and noise performance compared to MODIS and thus cannot be used to directly validate MODIS. Because the MAS cloud detection algorithm is essentially the same as the MODIS, we use the MAS to assess the capability of the algorithm approach to detecting clouds.

Comparisons were made using the ER-2-borne Cloud Physics Lidar (CPL) and collocated observations of the MAS (King et al. 1996). The CPL, developed by NASA Goddard Flight Space Center, flies on the ER-2 high-altitude aircraft (McGill et al. 2002). The CPL is an active remote sensing system, capable of high vertical resolution cloud height determinations (30 m), cloud visible optical depth, and backscatter depolarization. The CPL laser transmits at 355, 532, and 1064 nm and fires 5000 shots per second. The high sample rate of the CPL results in a surface footprint that can be approximated as a continuous line with a diameter of 2 m. The MAS is a scanning spectrometer with a 2.5-mrad

field of view. The MAS scene mirror scans at 7.25 Hz with a swath width of 42.96° from nadir resulting in a 50-m nadir surface resolution with a swath width of 37.2 km at the 20-km ER-2 flight altitude (King et al. 1996). The MAS has 50 spectral channels located within the 0.55–14.2- μm spectral region.

The MODIS cloud detection algorithm was based on using the MAS observations as proxy to the MODIS, as discussed by Ackerman et al. (1998). The collocation of these datasets is discussed in Holz et al. (2006). Because CPL is a nadir-only measurement, just MAS nadir IFOVs are compared for this investigation. To explore the optical depth sensitivity, we consider those cases in which the MAS detects clear sky and the lidar detects a cloud, and we analyze the lidar-retrieved optical depth. Figure 12 shows the number of occurrences where the MAS scene was identified as clear and the cloud physics lidar (McGill et al. 2002) detected a cloud as a function of the visible optical depth. This analysis suggests that a minimum requirement for cloud detection as defined by optical depth is approximately 0.4, as clouds with smaller optical depths are often classified as clear. To explore this further, we consider a comparison with the HSRL.

The HSRL observes both the Rayleigh and Mie (i.e., molecular and aerosol) backscatter simultaneously in two separate channels. The addition of a molecular channel, where the backscattering cross section is

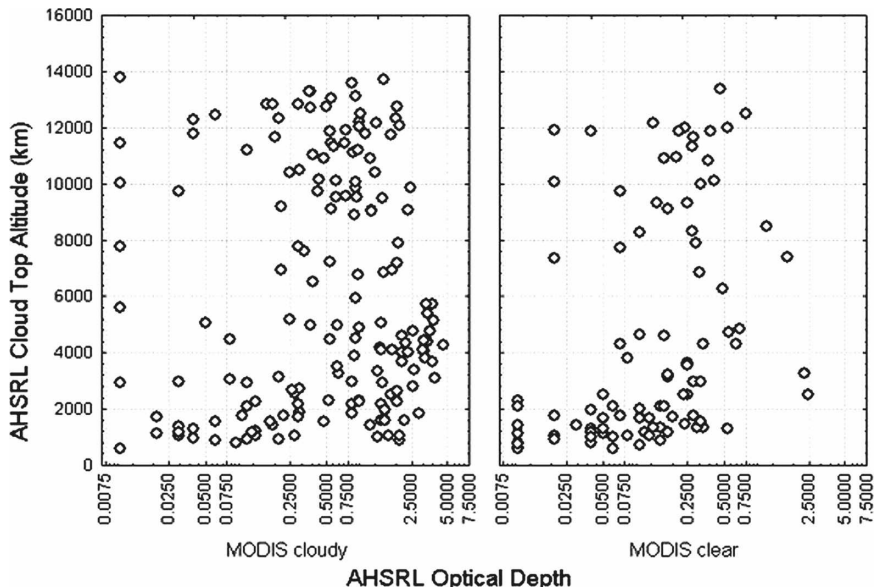


FIG. 13. (left) Scatterplot of AHSRL optical depth vs AHSRL cloud-top altitude for cases where AHSRL and MODIS detected cloudy. (right) Scatterplot of AHSRL optical depth vs AHSRL cloud-top altitude for cases where AHSRL detected a cloud and MODIS cloud mask indicated clear. The time period for both is January–August in Madison in 2004, for both *Terra* and *Aqua* overpasses.

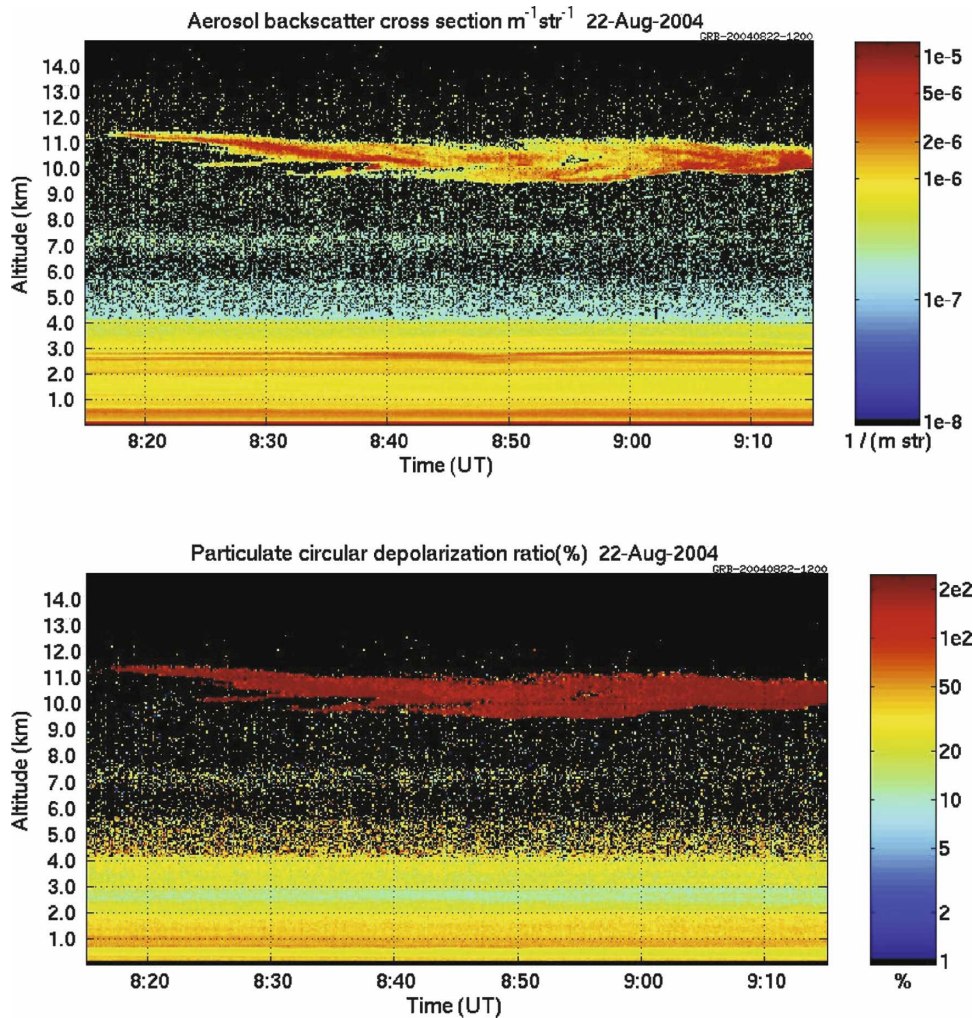


FIG. 14. (top) AHSRL cloud and aerosol backscatter and (bottom) depolarization ratio on 22 Aug 2004 over Madison between 0815 and 0905 UTC. The MODIS overpass at approximately 0839 UTC indicated a clear scene. The total cloud/aerosol optical depth as measured by the AHSRL is approximately 0.2.

known, allows the cloud extinction profile to be derived directly from the observations without assumptions. The HSRLs observe cloud extinction profiles with a high spatial and temporal resolution, a capability that makes HSRL observations unique and very powerful for investigating the MODIS cloud mask sensitivity to cloud optical depth. The University of Wisconsin—Madison has pioneered the advancement of HSRLs over the last three decades (e.g., Eloranta 2005). The current Arctic-HSRL (AHSRL) provides time histories of the following cloud and aerosol variables: 1) optical depth profiles as a function of altitude; 2) circular depolarization profiles as a function of altitude, which allows discrimination between ice crystals and water droplets; 3) backscatter cross section as a function of altitude; 4) cloud-base altitude; and 5) cloud-top alti-

tude for clouds of optical depths less than approximately 2.5. Raw data are acquired at 7.5-m range intervals with 0.5-s time resolution. All vertical profiles begin at an altitude of 100 m and extend to 30 km. A cloud is considered to occupy a layer when the aerosol backscatter cross section is greater than $1 \times 10^{-6} (m \text{ sr})^{-1}$. When dense clouds are present, useful data will be present up to an altitude where the optical depth reaches approximately 2.5.

The AHSRL was operated at Madison, Wisconsin, in an automated manner during January–September 2004. Table 3 shows the comparison between MODIS cloud detection and the AHSRL, including day and night cases for both *Terra* and *Aqua* satellites. The two cloud detection methods agree approximately 70% of the time. Figure 13 is a scatter diagram of AHSRL optical

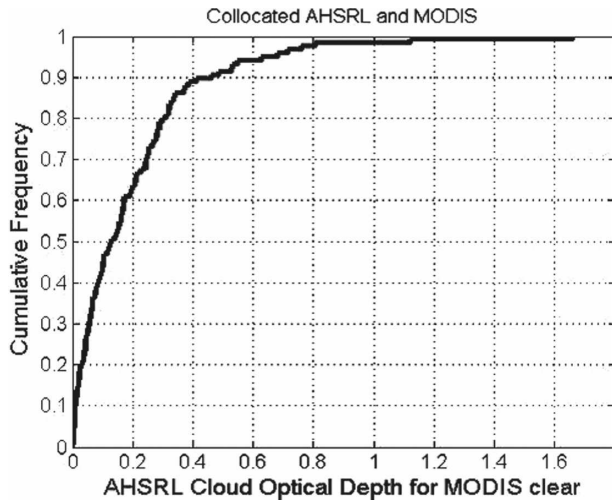


FIG. 15. The cumulative frequency of optical depth when a MODIS pixel was identified as clear by the MODIS cloud mask algorithm but the AHSRL detected a cloud with a given cloud optical depth for both *Terra* and *Aqua* overpasses between January–August in Madison.

depth versus AHSRL-determined cloud top for MODIS cloudy (Fig. 13, left) and clear scenes (Fig. 13, right). While there are cases when MODIS detects clouds for AHSRL optical depths less than 0.4, much of the disagreement between the AHSRL and MODIS occurs for optical depths less than 0.4. Figure 14 presents an example of optically thin cirrus, where MODIS labels the scene as clear and AHSRL detects cloud. The observation is for 22 August 2004, and the MODIS views the AHSRL region at approximately 0839 UTC. During this time, the AHSRL is clearly detecting an optically thin cloud with an optical depth less than 0.1 at approximately 10 and 11.5 km along with an aerosol layer near the surface. The total optical depth of the cloud/aerosol column is 0.2 with the aerosol optical depth contributing approximately three-quarters of the total optical depth. The MODIS cloud mask does not have sensitivity to this thin cirrus.

Figure 15 is the cumulative frequency of AHSRL optical depth for when collocated MODIS detects a clear scene. Of those cases where the lidar detected a cloud or aerosol and MODIS indicated clear, more than 60% of the time the optical depth was less than 0.2 and 90% of the time the nonmolecular optical depth was less than 0.4.

We next compare the MODIS cloud detection over the Arctic with observations from the Geoscience Laser Altimeter System (GLAS). Polar regions at night are the most challenging scenes in which to detect clouds with passive radiometers (e.g., Liu et al. 2004).

c. GLAS satellite observations

The launch of GLAS on board the Ice, Cloud, and Land Elevation Satellite (ICESat; Zwally et al. 2002) platform in January 2003 provides space-borne laser observations of atmospheric layers. Mahesh et al. (2004) compared GLAS cloud observations with an earlier version of the MODIS cloud mask and found that in more than three-quarters of the cases, MODIS scene identification agreed with GLAS. Disagreement between the two instruments was largest over snow-covered surfaces in the Northern Hemisphere, and MODIS cloud detection with sunlit observations was more robust than observations made at night.

The comparison in this study uses MODIS *Terra* Collection 5 cloud mask data from the period 16 October–18 November 2003. The MODIS data were aggregated from level 2 (5-min granule) files while the GLAS were averaged from medium-resolution daily values. The time period coincides with that of the fully functional 532-nm channel on the GLAS. MODIS spatial resolution is 1 km and GLAS is about 70 m across-track \times 7000 m along-track (one result per second). Both datasets were sorted into 2.5° equal-area grids, then converted to equal-angle grids for display purposes. MODIS and GLAS mean cloud amounts are compared for 2.5° equal-area grid cells in the Arctic. MODIS cloud fractions for this region are shown in Fig. 16 along with MODIS minus GLAS cloud frequencies. The GLAS detects more clouds for most grid cells, especially over the Arctic Ocean and the Greenland ice sheet, where reduced visible and thermal contrast make cloud detection more difficult for passive retrievals. This comparison includes all MODIS observations, so there are times when MODIS indicates a large cloud amount, which results from a combination of different measurements but also the nadir-only viewing of the GLAS. Differences are largest north of the Laptev Sea and the East Siberian Sea, where differences are larger than -30% . An analysis of the distribution of MODIS minus GLAS cloud fractions indicates a mode of -10% .

The GLAS is nadir-viewing only and given that cloud detection is a function of view angle (see Fig. 9), a comparison with only nadir views of MODIS was conducted. The impact of including only nadir views is shown in Fig. 17; zonal mean MODIS and GLAS cloud fraction differences for the time period are plotted. The differences are approximately -5% for the daylight regions of this comparison and become as large as -20% for regions that lack solar illumination. The comparison shown in Fig. 17 includes all MODIS pixels as well as

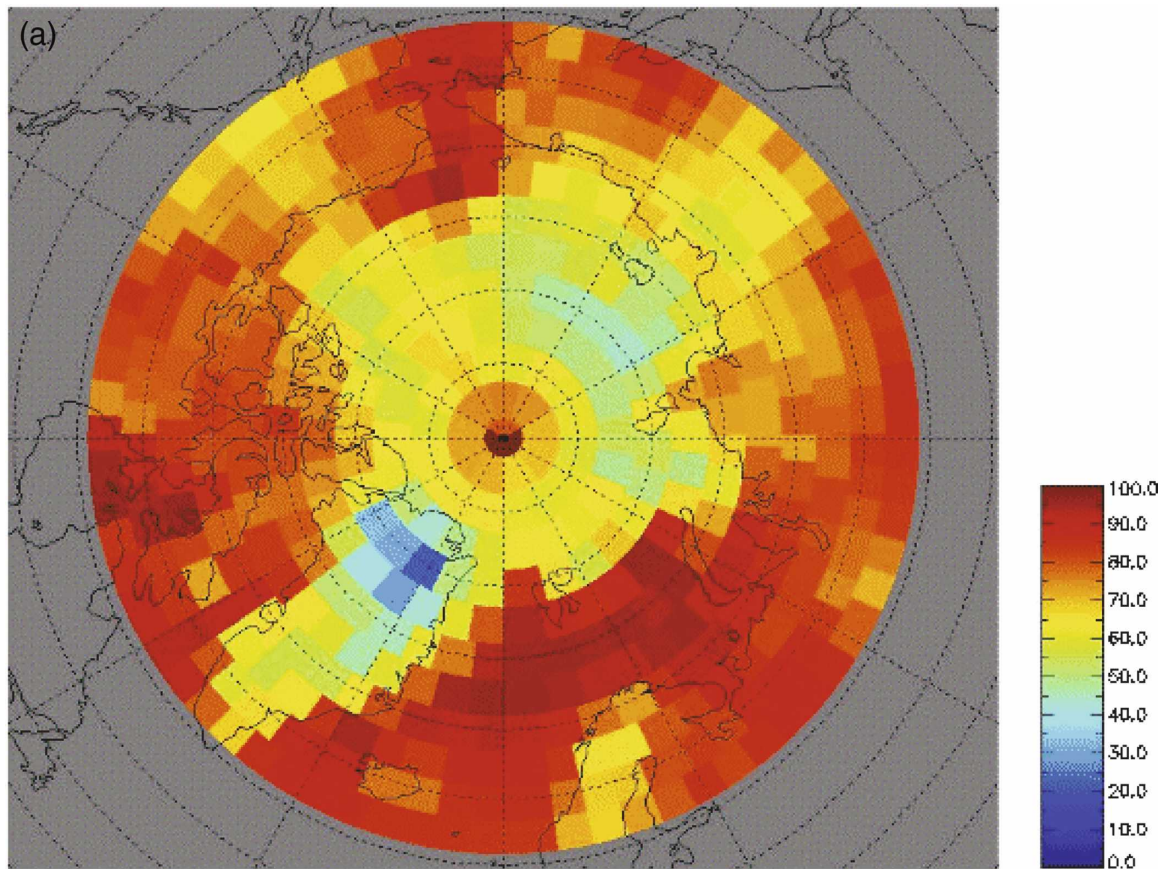


FIG. 16. (a) MODIS *Terra* Collection 5 cloud frequency from 60°–90°N. (b) MODIS minus GLAS cloud frequency. GLAS data product is the medium-resolution (one value per second) cloud frequency.

nadir only, defined as the middle two pixels of each scan line. Including only nadir pixels reduces the MODIS cloud cover by approximately 5%, worsening the agreement with GLAS. The results of this comparison with GLAS are similar, though slightly better than the earlier study of Mahesh et al. (2004).

5. Summary

This paper provides a comprehensive study of the cloud detection capability of the MODIS cloud mask algorithm. Validation was conducted through comparison with active observing systems that are generally more sensitive to the presence of clouds; however, the ground-based observations do not allow an assessment of the cloud detection capability for all scene types. The comparisons with four different lidar systems can be summarized as follows:

- Agreement between MODIS and the ARSCL for both cloud and clear scenes is approximately 85%.
- Comparison with GLAS during 16 October–18 No-

vember 2003 indicates that issues remain with cloud detection over polar regions during night. A more detailed analysis with the Cloud-Aerosol Lidar and Infrared Pathfinder Satellite Observation (CALIPSO) is under way.

- Through a comparison with cloud optical depths measured by a ground-based Arctic High-spectral Resolution lidar (HSRL), the MODIS cloud mask algorithm appears most sensitive to clouds with an optical depth greater than 0.4. This is consistent when an analogy is drawn with the CPL and MAS analysis on the ER-2.

The paper also demonstrates the sensitivity of the cloud-masking approach to various thresholds and conditions. Nadir-viewing sampling generally yields less cloud amount regionally than does the use of an entire swath, and a small IFOV generally detects more clear-sky scenes. Over clear-sky, sun-glint-free ocean, the reflection test at 0.86 μm detects nearly all the clouds found by the complete algorithm. Because many satellites have this channel, it would be a valuable exer-

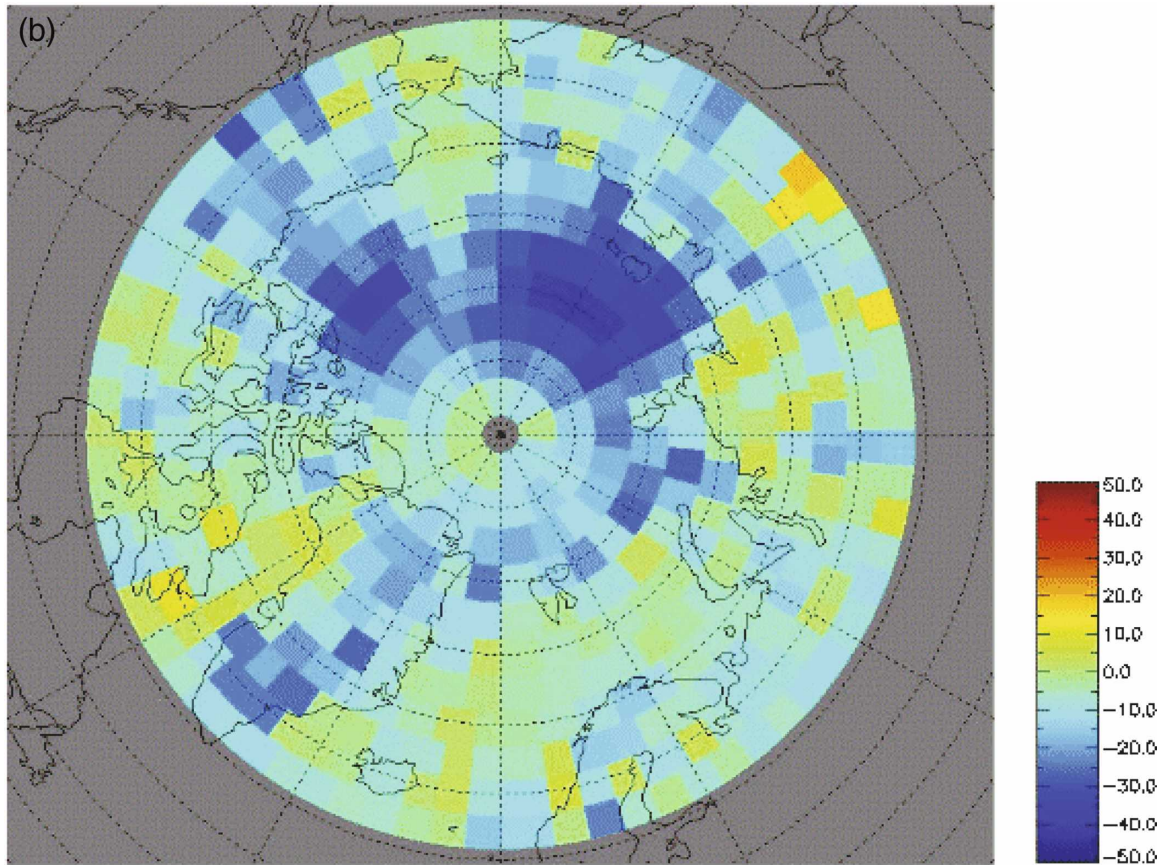


FIG. 16. (Continued)

ise for various cloud detection algorithms to compare cloud amounts using only this test to understand the impacts of various instrument-sampling characteristics.

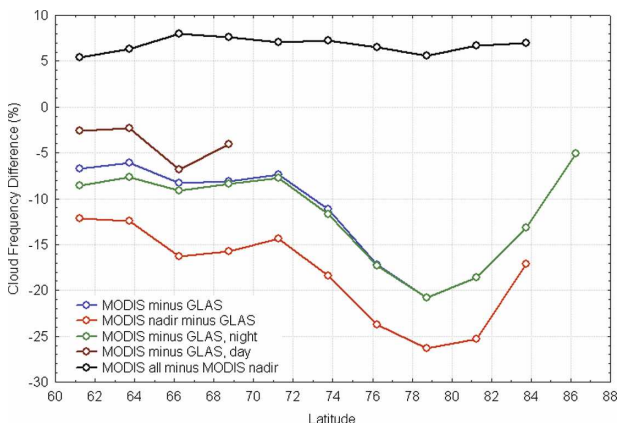


FIG. 17. MODIS and GLAS cloud fraction differences. North of approximately 76° latitude “all” and “night” categories are the same due to the season. Nadir MODIS data represent the two MODIS pixels near nadir, day, and night combined.

Acknowledgments. This research was funded under NASA Grants NNG04HZ38C and NNG04GL14G; NNG04GB93G also contributed to this study. The authors continue to appreciate the support provided by the MODIS Characterization and Support Team and the MODIS Science Data Support Team. These research efforts have been supported by a number of agencies and research programs; a particular acknowledgement is due the NASA Radiation Sciences Program and the NASA Earth Observing System Project Science Office. Thanks to the MODIS science team for many fruitful discussions. DOE ARM SGP site ARSCL data were obtained from the Atmospheric Radiation Measurement (ARM) Program sponsored by the U.S. Department of Energy, Office of Science, Office of Biological and Environmental Research, Environmental Sciences Division.

REFERENCES

Ackerman, S. A., K. I. Strabala, W. P. Menzel, R. A. Frey, C. C. Moeller, and L. E. Gumley, 1998: Discriminating clear sky from clouds with MODIS. *J. Geophys. Res.*, **103**, 32 141–32 157.

- Barnes, W. L., T. S. Pagano, and V. V. Salomonson, 1998: Pre-launch characteristics of the Moderate Resolution Imaging Spectroradiometer (MODIS) on EOS-AM1. *IEEE Trans. Geosci. Remote Sens.*, **36**, 1088–1100.
- Clothiaux, E. E., T. P. Ackerman, G. G. Mace, K. P. Moran, R. T. Marchand, M. A. Miller, and B. E. Martner, 2000: Objective determination of cloud heights and radar reflectivities using a combination of active remote sensors at the ARM CART sites. *J. Appl. Meteor.*, **39**, 645–665.
- Di Girolamo, L., and R. Davies, 1997: Cloud fraction errors caused by finite resolution measurements. *J. Geophys. Res.*, **102**, 1739–1756.
- Eloranta, E. W., 2005: High spectral resolution lidar. *Lidar: Range-Resolved Optical Remote Sensing of the Atmosphere*, K. Weitkamp, Ed., Springer Series in Optical Sciences, Springer-Verlag, 143–163.
- Frey, R. A., S. A. Acherman, Y. Liu, K. I. Strabala, H. Zhang, J. R. Key, and X. Wang, 2008: Cloud detection with MODIS. Part I: Improvements in the MODIS cloud mask for Collection 5. *J. Atmos. Oceanic Technol.*, **25**, 1057–1072.
- Holz, R. E., S. A. Ackerman, P. Antonelli, F. Nagle, B. O. Knutson, M. McGill, D. L. Hlavka, and W. D. Hart, 2006: An improvement to the high-spectral-resolution CO₂-slicing cloud-top altitude retrieval. *J. Atmos. Oceanic Technol.*, **23**, 653–670.
- King, M. D., and Coauthors, 1996: Airborne scanning spectrometer for remote sensing of cloud, aerosol, water vapor, and surface properties. *J. Atmos. Oceanic Technol.*, **13**, 777–794.
- , and Coauthors, 2003: Cloud and aerosol properties, precipitable water, and profiles of temperature and humidity from MODIS. *IEEE Trans. Geosci. Remote Sens.*, **41**, 442–458.
- Klein, S. A., and D. L. Hartmann, 1993: The seasonal cycle of low stratiform clouds. *J. Climate*, **6**, 1587–1606.
- Lee, Y., G. Wahba, and S. A. Ackerman, 2004: Cloud classification of satellite radiance data by multcategory support vector machines. *J. Atmos. Oceanic Technol.*, **21**, 159–169.
- Li, Z., J. Li, W. P. Menzel, T. J. Schmit, and S. A. Ackerman, 2007: Comparison between current and future environmental satellite imagers on cloud classification using MODIS. *Remote Sens. Environ.*, **108**, 311–326.
- Liu, Y., J. Key, R. Frey, S. Ackerman, and W. Menzel, 2004: Nighttime polar cloud detection with MODIS. *Remote Sens. Environ.*, **92**, 181–194.
- Mahesh, A., M. A. Grey, S. P. Palm, W. D. Hart, and J. D. Spinhirne, 2004: Passive and active detection of clouds: Comparisons between MODIS and GLAS observations. *J. Geophys. Res.*, **108**, L04108, doi:10.1029/2003GL018859.
- McGill, M., D. Hlavka, W. Hart, V. S. Scott, J. D. Spinhirne, and B. Schmid, 2002: Cloud physics lidar: Instrument description and initial measurement results. *Appl. Opt.*, **41**, 3725–3734.
- Minnis, P., 1989: Viewing zenith angle dependence of cloudiness determined from coincident GOES East and GOES West data. *J. Geophys. Res.*, **94**, 2303–2320.
- , and E. F. Harrison, 1984: Diurnal variability of regional cloud and clear-sky radiative parameters derived from GOES data. Part II: November 1978 cloud distributions. *J. Climate Appl. Meteor.*, **23**, 1012–1051.
- , P. W. Heck, D. F. Young, C. W. Fairall, and J. B. Snider, 1992: Stratocumulus cloud properties derived from simultaneous satellite and island-based instrumentation during FIRE. *J. Appl. Meteor.*, **31**, 317–339.
- Platnick, S., M. D. King, S. A. Ackerman, W. P. Menzel, B. A. Baum, J. C. Riedi, and R. A. Frey, 2003: The MODIS cloud products: Algorithms and examples from Terra. *IEEE Trans. Geosci. Remote Sens.*, **41**, 459–473.
- Rossow, W. B., 1989: Measuring cloud properties from space. A review. *J. Climate*, **2**, 201–213.
- , A. W. Walker, and L. C. Gardner, 1993: Comparison of ISCCP and other cloud amounts. *J. Climate*, **6**, 2394–2418.
- Stokes, G. M., and S. E. Schwartz, 1994: The Atmospheric Radiation Measurement (ARM) Program: Programmatic background and design of the cloud and radiation test bed. *Bull. Amer. Meteor. Soc.*, **75**, 1201–1221.
- Thomas, S. M., A. K. Heidinger, and M. J. Pavolonis, 2004: Comparison of NOAA's operational AVHRR-derived cloud amount to other satellite-derived cloud climatologies. *J. Climate*, **17**, 4805–4822.
- Wylie, D. P., W. P. Menzel, H. M. Woolf, and K. I. Strabala, 1994: Four years of global cirrus cloud statistics using HIRS. *J. Climate*, **7**, 1972–1986.
- Zhao, G., and L. Di Girolamo, 2006: Cloud fraction errors for trade wind cumuli from EOS-Terra instruments. *Geophys. Res. Lett.*, **33**, L20802, doi:10.1029/2006GL027088.
- Zwally, H. J., and Coauthors, 2002: ICESat's laser measurements of polar ice, atmosphere, ocean, and land. *J. Geodyn.*, **34**, 405–445.